

X-RAY IRRADIATED PROTOPLANETARY DISK ATMOSPHERES I: PREDICTED EMISSION LINE SPECTRUM AND PHOTOEVAPORATION

BARBARA ERCOLANO^{1,2}, JEREMY J. DRAKE², JOHN C. RAYMOND², CATHIE C. CLARKE¹

¹Institute of Astronomy, University of Cambridge,
Madingley Rd,
Cambridge, CB3 0HA, UK

²Harvard-Smithsonian Center for Astrophysics, MS-67
60 Garden Street,
Cambridge, MA 02138, USA

Accepted by ApJ

ABSTRACT

We present MOCASSIN 2D photoionisation and dust radiative transfer models of a prototypical T Tauri disk irradiated by X-rays from the young pre-main sequence star. The calculations demonstrate a layer of hot gas reaching temperatures of $\sim 10^6$ K at small radii and $\sim 10^4$ K at a distance of 1 AU. The gas temperatures decrease sharply with depth, but appear to be completely decoupled from dust temperatures down to a column depth of $\sim 5 \times 10^{21} \text{ cm}^{-2}$.

We predict that several fine-structure and forbidden lines of heavy elements, as well as recombination lines of hydrogen and helium, should be observable with current and future instrumentation, although optical lines may be smothered by the stellar spectrum. Predicted line luminosities are given for the the brightest collisionally excited lines (down to $\sim 10^{-8} L_{\odot}$), and for recombination transitions from several levels of H I and He I.

The mass loss rate due to X-ray photoevaporation estimated from our models is of the order of $10^{-8} M_{\odot} \text{ yr}^{-1}$, implying a dispersal timescale of a few Myr for a disk of mass $0.027 M_{\odot}$, which is the mass of the disk structure model we employed. We discuss the limitations of our model and highlight the need for further calculations that should include the simultaneous solution of the 2D radiative transfer problem and the 1D hydrostatic equilibrium in the polar direction.

Subject headings: Accretion, Accretion Disks, Infrared: Stars, Stars: Planetary Systems: Protoplanetary Disks, Stars: Formation, Stars: Pre-Main-Sequence, X-Rays: Stars

1. INTRODUCTION

Protoplanetary disks are a product of the formation of protostars from the collapse of molecular cloud cores. These disks remain a source of ongoing accretion for the central stellar object for a period of up to ~ 10 Myr (Manning & Sargent, 1997; Wyatt, Dent & Greaves, 2003) and are the birthplaces of planetary systems. The evolution of the disk and of its planetary progeny is controlled by heating and irradiation from the central star—from IR to X-rays—but in the vicinity of OB stars can also be significantly affected by the external radiation environment (e.g. Johnstone et al. 1998; Adams et al., 2004; Fatuzzo & Adams, 2008).

The discovery of the “proplyd” phenomenon and subsequent observations of protoplanetary disks represent an important and growing part of the legacies of the *Hubble* and *Spitzer* space telescopes (e.g. O’Dell 1993, Bally et al. 1998, Evans et al. 2003, Meyer et al. 2004). New instruments such as the *Mid-Infrared Instrument* on board *James Webb Space Telescope*, which will provide both imaging and spectroscopy, hold the promise for higher spatial resolution. On the ground, millimeter and submillimeter studies have evolved from examining disk size and orientation (e.g. Keene & Masson 1990, Lay et al. 1994) to detailed studies of structure, chemistry and thermal properties (e.g. Wilner et al. 2003, Qi et al. 2006), while future high spatial resolution submillimeter observations with ALMA promise further major advances (e.g. van Dishoeck & Jørgensen 2008).

These and other observations should provide insights into issues central to understanding disks and the likelihood of forming planetary systems like our own, such as angular momentum transport, and the timescales for grain growth and gas dissipation. Of particular interest for interaction of the disk with its parent star and for the study of planetary origins are the inner regions of disks (≤ 10 AU) where both terrestrial and giant planets are believed to form.

While the observational database continues to grow, all attempts at theoretically modeling the emission expected from such environments have lacked several of the ingredients needed for a fully self-consistent approach. The multidimensional, far-Ultra Violet (UV) to X-ray radiative transfer (RT) problem must be solved simultaneously with the disk hydrodynamical evolution, to which it is strongly coupled. Furthermore, disks comprise adjacent regions of ionised, photon-dominated and molecular gas intermixed with a non-uniform dust component. No computer code currently available includes all the important physics and chemistry needed to properly interpret the observational diagnostics of these different regimes. Furthermore, full theoretical understanding of a number of important contributors to the energetics of the system, such as accretion and wind-disk interactions, is still lacking; these ingredients can currently only be included through approximate and phenomenological approaches (e.g. see discussion in Glassgold et al., 2004).

Several studies have focused on the properties of the dust component of disk atmospheres (e.g. D’Alessio et

al. 2001, Dullemond et al. 2002, Akeson et al 2005). However, studies of the gaseous component of the inner disks have only recently been attempted, and only an exploratory picture of the thermochemical structure of this crucial component has emerged. Pioneering work from Igea & Glassgold (1999), Glassgold et al., (2004, 2005) and Meijerink et al. (2008) examined physical conditions and expected emission lines in the gaseous component of non-evolving T Tauri disks irradiated by X-rays. Nomura & Millar (2005) modeled molecular hydrogen emission from protoplanetary disks, taking into account UV radiation from a central star; their models, while calculating the density and temperature structures self-consistently, did not account for X-radiation and employed an approximate treatment of the scattered light that often leads to an overestimation of the UV radiation field in the disk (Glassgold, 2006). Semenov et al. (2004) employed perhaps the most complete chemical network to date to calculate the ionisation fractions at the disk midplane. While X-ray ionisation was included, radiative transfer through scattering and diffusion was not. Simple column density arguments were used instead to estimate the radiation field attenuation at discrete points in the disk where the chemical model was applied. Very recently Gorti & Hollenbach presented 1+1D models of gas in optically thick disks, calculating thermal, density and chemistry structures, with special attention to the effects of FUV irradiation.

More detailed 2D or 3D calculations are now needed to provide a quantitative picture of these environments in relation to their effects on the disk spectral energy distribution (SED), and on other observables available now and in the near future (e.g. [O I], [Ne II], CO, OH, and UV transitions of H₂; Najita et al, 2007). In particular, observations of forbidden lines in T Tauri stars provide evidence for a tenuous, hot outer layer, or ‘corona’ (Kwan & Tademaru 1988, 1995; Kwan (1997). The earlier work by Glassgold et al. (2004, 2007), Semenov et al. (2004) and Meijerink et al. (2008) emphasised the chemistry in the photo-dissociation region (PDR) and molecular zones, and stopped short of this coronal layer. Also the recent work by Gorti & Hollenbach does not include the fully ionized layer discussed here.

In this paper, which is the first of a series aimed at building a more realistic and self-consistent model of irradiated gaseous T Tauri disks, we employ a fully 3D photoionisation and dust radiative transfer code, MOCASSIN (Ercolano et al., 2003, 2005, 2008), to calculate the detailed ionisation and temperature structure of a typical T Tauri disk, with special emphasis on the photoionisation-dominated outer layers and corona. We show that hot coronal temperatures are expected from X-ray irradiation from the central pre-main sequence star. Our calculations aim to understand the thermochemical structure of the irradiated region and to identify emission lines that can be used as gas-phase diagnostics for current and future observations. Furthermore, the detailed 2D temperature structure calculated by our models allows us to estimate the efficiency of X-radiation to drive a photoevaporative wind.

Our model is described in Section 2. The ionisation and temperature structures are presented and discussed in Section 3, while the predicted emission line spectra are shown in Section 4. Section 5 contains a discussion

of our results in the context of disk dispersal via X-ray photoevaporation. A brief summary is given in Section 6.

2. THE 2D MONTE CARLO PHOTOIONISATION AND DUST RADIATIVE TRANSFER MODEL

Photoionisation and temperature structure calculations were performed with Version 3.02.00 of the 3D Monte Carlo photoionisation and dust radiative transfer code, MOCASSIN (Ercolano et al. 2003, 2005, 2008). The code uses a stochastic approach to the transfer of radiation allowing for the self-consistent transfer of both the primary and secondary components of the radiation field. The code was modified to include viscous heating, approximated using the prescription for a thin disk by Pringle (1981), and gas cooling by collisions of grains with a mixture of atomic and molecular hydrogen (Hollenbach & McKee, 1979); we discuss this further below. MOCASSIN was also adapted to run in 2D, using the gas and dust density distribution given by a 2D protoplanetary disk calculation of D’Alessio et al. (1999).

The D’Alessio model used in our calculation was chosen to be that which best fits the median SED of T Tauri stars in Taurus (d’Alessio, 2005). We refer the reader to D’Alessio et al. (1999) for a detailed description of the model ingredients and calculation. In brief, the input parameters for this model include a central star of $0.7 M_{\odot}$, $2.5 R_{\odot}$ irradiating the disk with an effective temperature of 4000 K. Additional disk parameters consist of a mass accretion rate of $1.e-8 M_{\odot} \text{ yr}^{-1}$ and a viscosity parameter $\alpha = 0.01$. The total mass of the disk is $0.027 M_{\odot}$.

The present study is particularly focused on determining the physical properties of the gas in the outer layers and hot disk corona. Molecular species that are expected to form deeper in the disk are not included in our model; this poses a limitation on the accuracy of our gas temperature calculations in the inner layers. In particular, the calculations by Glassgold et al., (2004, GNI04) have shown that CO rovibrational lines may become important coolants, and, e.g., at a radial distance of 1 AU and column densities of 10^{21} - 10^{22} cm^{-2} CO was found to dominate the disk cooling. CO rotational lines are also expected to form at greater depths, though in these regions the thermal balance is dominated by dust-gas collisions (GNI04).

Dust-gas collisions can heat the gas/dust if the gas is cooler/warmer than the dust; photoelectric emission from dust grains heats the gas and it provides a minor cooling channel for the dust. MOCASSIN is able to self-consistently calculate the dust and gas thermal balance, taking into account the main microphysical processes that couple the two phases. Here, however, we choose to keep the dust temperatures fixed to the values calculated by D’Alessio et al. (1999) and focus our discussion on the gas phase. In the current work we do not treat the transfer of the stellar or interstellar far-UV field, and therefore the dust temperatures we would obtain from our models would be incorrect. The effects of gas-dust interactions on the temperature structure of the gas, however, are still taken into account in our gas thermal balance as well as in the radiative transfer, where the competition between dust and gas for the absorption of X-ray radiation is properly treated.

We illuminate the disk using synthetic X-ray spec-

tra representative of the high energy emission from a typical T Tauri star. There are currently at least three different mechanisms by which T Tauri stars are thought to produce observable X-rays: magnetospheric accretion shocks, shocks resulting from polar jets, and magnetically-confined hot coronae analogous to those found on all late-type main-sequence stars including the Sun (e.g. Kastner et al 2002, Güdel et al 2005, Walter & Kuhl, 1981). The first two of these have only been identified in a small handful of stars, and since the latter appears to dominate the observed X-ray spectra of T Tauri stars we currently ignore the effects of X-rays from jets and accretion.

Coronal X-ray emission arises from an optically-thin plasma dominated by impact excitation and ionization by thermal electrons. The spectra from such a plasma comprises significant contributions from bound-bound, bound-free and free-free radiation. We computed synthetic coronal spectra incorporating these processes for the energy range 13.6 eV-12.5 keV for all elements with atomic number $Z=1$ to 30 using line and continuum emissivities from the CHIANTI compilation of atomic data (Landi et al., 2006, and references therein), together with ion populations from Mazzotta et al. (1998), as implemented in the PINTofALE IDL software suit¹ (Kashyap & Drake, 2000). We adopted the solar chemical composition of Grevesse & Sauval (1998) for the calculated spectra and an X-ray temperature, $\log(T_x) = 7.2$. We assume an X-ray luminosity, $L_X(0.1-10 \text{ keV}) = 2 \times 10^{30} \text{ erg/sec}$.

Details on atomic data and physical processes used for the photoionisation calculations are given by Ercolano et al. (2003, 2008) and Ercolano & Storey (2006). The chemical composition of Grevesse & Sauval (1998) was also used for the gas abundances of the most common elements used in our photoionisation model of the disk corona. In view of the ongoing debate on the ‘‘solar oxygen crisis’’ (e.g. Ayres et al. 2006; Drake & Testa, 2005; Socas-Navarro & Norton, 2007; Socas-Navarro & Centeno, 2008), we have chosen not to use the more recent compilations of solar abundances based on 3-D non-LTE hydrodynamic photospheric modeling (e.g. Asplund et al. 2005), which recommends 25-35% lower C, N, O and Ne abundances compared to earlier assessment. We also ignore the possible effects of grain depletion. Although some depletion of refractory elements onto dust grains is expected, the amounts are very uncertain and probably quite small in the disk corona where the X-ray field is more intense. Here, undepleted values of C, Mg, Si and Fe abundances correspond to efficient destruction of grains in the upper layers of the disk. A test for the validity of this assumption could be provided by the Si II 34.8 μm line, which is a good diagnostic for grain depletion, and which our models predict to be observable (see Table 1).

The dust absorption and scattering coefficients are calculated for high energies using the dielectric constants for graphite and silicates of Laor & Draine (1993), which extend to the X-ray domain. We assume spherical grains and use standard Mie scattering series expansion for $x|m| < 1000$, where m is the complex refractive index and $x = 2 \cdot a/\lambda$ is the scattering parameter (see Laor

& Draine, 1993). For $x|m| > 1000$ and $x|m - 1| < 0.001$ we use Rayleigh-Gans theory (Bohren & Huffman, 1983), and for $x|m| > 1000$ and $x|m - 1| > 0.001$ we use the treatment specified by Laor & Draine (1993), which is based on geometric optics.

Our dust model consists of a typical ISM mixture of graphite and silicates with MRN size distribution (Mathis, Rumpl & Nordsieck, 1977) described by $a_{min} = 0.005\mu\text{m}$ and $a_{max} = 0.25\mu\text{m}$. The chosen grain size distribution does not take into account grain growth, and therefore over-emphasizes the cooling of the gas by the dust in the disk interior. We also assume a dust to gas mass ratio of 0.01 throughout the disk. We note that the density distribution model of D’Alessio et al. (1999) uses different dust prescriptions at different heights, in order to account for the effects of grain settling and growth. For the sake of simplicity, and because we assume the dust temperatures calculated by D’Alessio et al. (1999), we chose to use a more standard dust model throughout our disk. Since matching a particular SED is not one of our main objectives, and we are mostly interested in the physical properties of the disk corona, the choice of the size distribution and species is not crucial in our work as it will only have a very small effect on the ionisation and temperature structure of the coronal gas.

As noted earlier, in addition to all the standard heating and cooling channels included in MOCASSIN, we also include viscous accretion heating calculated assuming the standard dissipation rate for a thin disk (Pringle, 1981)

$$\Gamma_{acc} = \frac{9}{4} \alpha \rho c_s^2 \Omega \quad (1)$$

where ρ is the local mass density of the gas, c_s is the isothermal sound speed and Ω is the angular rotation speed. The parameter $\alpha = 0.01$ relates viscous heating to the gas pressure.

The formulation above is purely phenomenological and carries large uncertainties. In particular, the appropriate value of α is unclear when the formula is applied to the warm disk atmosphere (GNI04), where it is unknown if angular momentum transport such as the magneto-rotational instability (MRI; Balbus & Hawley, 1991) even operates at all. GNI04 show the effect that varying the value of α has on the temperature structure of the gas, but finally adopt a model with $\alpha = 0.01$ for their line emission predictions (Glassgold et al. 2007; Meijerink et al. 2008). A value of $\alpha = 0.01$ is also chosen by d’Alessio et al. (1998, 1999, 2001) for their disk structure calculations (which includes the model used in this paper). This choice is based on the connection between α and the disk accretion rate: $\dot{M}_D \propto \alpha \Sigma_D$, where Σ_D is the integrated surface density of the disk. With $\alpha = 0.01$, which is also the value implemented in our models, X-ray heating is dominant in the disk corona, while accretion heating dominates in the inner regions.

We finally note that the dependence of the heating rate on the square of the sound speed implies a *linear* dependence on the gas temperature, which poses potential problems for the hot disk corona. In the regions where the gas is heated to high temperatures by X-ray irradiation the functional form of accretion heating, as formulated above, fails completely, preventing an equilibrium temperature from being found. In fact, X-ray irradiation in the upper atmosphere of the inner regions

¹ Freely available from <http://hea-www.harvard.edu/PINTofALE>

of the disk heats the gas to temperatures above the local escape temperature of the gas (see section 5). The gas in these regions is to be considered unbound and part of a photoevaporative flow, hence not subject to the standard viscous accretion law. For unbound gas we remove the accretion heating contribution altogether by setting the local α coefficient to zero in our models.

3. THE IONISATION AND TEMPERATURE STRUCTURE

In this section, we present the temperature and ionisation structure of the gas in the inner disk, focusing our attention on the disk corona. We limit our discussion to radial distances $R \lesssim 40$ AU, beyond which, in our model, sets a rough outer limit to the region where the effects of X-ray irradiation on the temperature and ionisation structure are more evident. We note, however, that in our models a low levels of ionisation is maintained out to a radius of ~ 190 AU.

Figure 1 shows the temperature structure (asterisks) in the vertical column calculated at $R = 0.07$ AU, together with the dust temperature profile calculated by D’Alessio et al. (1999). Also shown is the volumetric gas density [cm^{-3}] as a function of depth, the corresponding geometrical height above the midplane is shown in the top x-axis. The gaseous disk corona at these very small radii is fully ionised. Since all elements are stripped of their outer electrons, cooling by collisionally excited lines is inefficient. The balance between heating by photoionisation and cooling by line emission and recombination processes corresponds to a gas equilibrium temperature of $\sim 10^6$ K.

At 0.07 AU, the jump in gas temperature occurs at a vertical column density of $\sim 5 \times 10^{14} \text{ cm}^{-2}$, where the gas density is $\sim 3 \times 10^4 \text{ cm}^{-3}$ and the ionisation parameter, defined as $\xi = L/nR^2$, is $\log(\xi) \sim 1.78$. This transition would look even sharper in a hydrostatically balanced model, since a rise in the temperature would induce a drop in density in order to maintain pressure equilibrium. In this case, any equilibria found in the 10^4 - 10^6 K range may in fact be unstable (Hatchett, 1976). This has already been noticed in accretion disk models around X-ray binaries (e.g. Raymond 1993). Alexander, Clarke & Pringle (2004, ACP04) have also presented a model to illustrate the effects of X-ray heating on the structure of circumstellar disks. In that work, the density profile was truncated at the point where the density fell to 10^4 cm^{-3} , which is below the fully ionised region shown in our Figure 1. This should be kept in mind when comparing our temperature structure to theirs (as shown in their Figure 3), where the lack of the $\sim 10^6$ K temperature (fully ionised) region is not surprising and is not discrepant with our results.

The electron density distribution, shown in Figure 2, indicates that the a high level of ionisation at 0.07 AU is maintained for a column density of 10^{17} cm^{-2} , after which it decays to lower values. A study of the thermal balance at this radius indicates X-ray heating dominates for a column depth of $\sim 10^{22} \text{ cm}^{-2}$, while heating by viscous accretion dominates further down in the disk where it is balanced by dust-gas collisional cooling. In our calculations, the contribution from accretion heating is set to zero in regions where X-ray irradiation heats up the gas to temperatures above the local escape temperature (see section 2). At $R = 0.07$ AU this occurs at a column

depth of $\sim 10^{14.5} \text{ cm}^{-2}$, at the onset of the temperature ‘discontinuity’.

Figure 3 shows the temperature and volumetric density [cm^{-3}] structures in the vertical column calculated at $R = 1$ AU, together with the D’Alessio et al. (1999) dust temperature profile. The coronal gas here appears to be only partially ionised and the electron density, illustrated in Figure 4, reaches a level of just over 10% of the hydrogen density, but decreases very rapidly with column depth.

Our temperature structure at 1 AU is comparable to that found by GNI04, allowing for differences in the model input parameters, and bearing in mind that their calculation started at a column depth of 10^{18} cm^{-2} . However, the cooling and heating contributions calculated by the two models disagree somewhat and deserve further explanation. The various heating and cooling channels in our model at 1 AU are illustrated as a function of vertical column depth in Figure 5, which can be compared with an analogous illustration in Figure 3 of GNI04. One conspicuous difference between the two models is the accretion heating contribution, which is simply due to the different choice of α (0.01 in this work and 1.0 in the particular model plotted in Figure 3 of GNI04). Note that GNI04, also investigated models with lower values of α (see their Figure 2), and indeed used a model with $\alpha = 0.01$, for their later work (Glassgold et al., 2007; Meijerink et al.; 2008), where emission line predictions are given. Unfortunately a plot showing the heating/cooling contributions from their models is only available for the $\alpha = 1$ case. Another important difference lies in the $\text{Ly}\alpha$ cooling contribution, which is only of secondary importance in our models but dominates the cooling down to a vertical column of 10^{21} cm^{-2} in the GNI04 model. The dominant cooling mechanism in the upper disk atmosphere in our model is metal line emission. The $\text{Ly}\alpha$ cooling in GNI04 was overestimated because of an assumption of a thermal equilibrium population for the $n = 2$ level. The “ $\text{Ly}\alpha$ ” channel in the GNI04 model also includes cooling by the fine structure lines of O I, while other atomic coolants are ignored. In spite of the aforementioned differences, the total cooling calculated by GNI04 is very similar to that obtained in this work for the regions where the calculations overlap and when the same α parameter is employed (Glassgold, 2008; private communication).

As we move to increasingly larger radii, up to approximately 25-30 AU, our model disk structure remains qualitatively similar to that at 1 AU: high gas temperatures are reached in the corona, followed by a steep temperature decrease, with the gas and dust becoming thermally coupled at a vertical column depth of $\sim 5 \times 10^{21} \text{ cm}^{-2}$. Beyond ~ 35 -40 AU, due to geometrical dilution of the central radiation field, the effects of X-ray irradiation become less evident, however a low level of ionisation is maintained out to a radius of ~ 190 AU. For T-Tauri stars born in clusters containing massive stars, like the Orion Nebula Cluster, the dominant irradiation mechanism at large disk radii is probably provided by the interstellar or intracluster FUV and X-ray fields, which are not included in our current models. This is not true for stars born in smaller clusters like ρ Ophiuchi and Taurus-Auriga, where indeed large disks (~ 500 -1000 AU) are found (Andrews & Williams, 2007).

The maximum temperature reached by the disk corona at a given radial distance is an immediate consequence of the local ionisation parameter. The fact that at 1 AU we do not see the $\sim 10^6\text{K}$ gas layer is simply due to the fact that the density distribution of d'Alessio et al. (1999) used in our models is truncated at a volumetric density of $\sim 10^4$. At 0.07 AU, the temperature jump to $\sim 10^6\text{K}$ occurs at a $\log(\xi) = 1.78$. The same value at 1 AU implies a density of $\sim 150\text{ cm}^{-3}$, which is below the cut-off.

The general results found in our models are similar to those found by Gorti & Hollenbach (2008), in particular that the gas and dust are thermally de-coupled down to a column of $\sim 10^{22}\text{ cm}^{-2}$.

4. PREDICTED EMISSION LINE SPECTRUM

As an aid to future observational campaigns, we have calculated the emission line spectrum predicted by our model. Line luminosities are integrated out to a radius of 190 AU. In Tables 1 and 2 we list a subset of the strongest collisionally excited metal line and hydrogen recombination lines, respectively, down to a luminosity of $\sim 10^{-8}\text{L}_\odot$, which corresponds to a flux of $\sim 1.8 \times 10^{-17}\text{ erg/s/cm}^2$ at a distance of 140pc. The flux at a distance D , assuming a face-on orientation for the disk, is obtained by dividing the luminosities listed by the appropriate dilution factor ($4\pi D^2$). He I recombination lines are found to be rather weak, with the exception of He I $10.8\mu\text{m}$ which has a luminosity of $8.8 \times 10^{-7}\text{L}_\odot$, He I 7067\AA with luminosity of $3.2 \times 10^{-8}\text{L}_\odot$ and He I 3890\AA , He I 5877\AA , He I 6688\AA and He I 20.5μ , all with luminosities of $\sim 2 \times 10^{-7}\text{L}_\odot$. The full set of lines, including over 2000 transitions is available on request from BE. The line list will be further improved and updated in a future work, when the effects of simultaneous stellar and interstellar FUV irradiation, as well as X-rays, will be considered. Some changes to the emission line intensities are also expected when the X-irradiation will be studied in the context of a self-consistent hydrostatic equilibrium calculation.

Tables 1 and 2 provide an indication of the lines that should be targeted for observations of the gaseous phase of disk atmospheres. A number of potential atomic and ionised gas diagnostic lines should already be detectable with current instrumentation. The [Ne II] $12.8\mu\text{m}$ line, in particular, has already been detected in T Tauri disks with *Spitzer* by Pascucci et al. (2007), Lahuis et al (2007) and Espaillat et al. (2007), and with MICHELLE on Gemini North by Herczeg et al. (2007). The detections to date range from a few 10^{-7} to 10^{-5} L_\odot , in qualitative agreement with values predicted by our model. The [Ne III] $15.5\mu\text{m}$ line has so far only been detected in Sz102 (Lahuis et al. 2007), implying a [Ne III]/[Ne II] of ~ 0.06 for this object, which is some 2.5 times larger than our model. As noted by Glassgold et al. (2007) the abundance of Ne^{2+} is lowered by charge exchange reactions with neutral H, implying low (≤ 0.1) ratios of [Ne III]/[Ne II] in the X-ray heated gas. Gorti & Hollenbach (2008) also discuss the effects of EUV irradiation which would enhance the predicted [Ne II] and [Ne III] line luminosities, and affect their ratio. They predict that the [Ne III]/[Ne II] also depends on the details of the EUV spectrum, with hard EUV spectra naturally producing the higher ratios.

Table 1 clearly shows that a number of optical lines have fluxes that are significantly larger than the [Ne II] $12.8\mu\text{m}$ fluxes. Unfortunately many optical and UV lines are not observable with current technology, as they are invisible against the stellar spectrum. In particular, we predict a luminosity of 3.3×10^{-5} for the Mg I line at 4573\AA , for undepleted Mg abundances. This corresponds to only a few % of the continuum flux level for a photosphere of 4000K and for an assumed resolving power of 50,000. While this line might be detectable under favourable circumstances and where disk gas is not strongly depleted, we are unaware of any such detections in the literature.

The predicted absolute flux of the various lines depends, of course, on the details of the disk structure, the gas abundances and the ionising spectrum. As an example, Meijerink et al. (2008, MGN08), show, for a fixed disk structure, the dependence of the predicted flux of a number of fine structure and forbidden lines on the assumed X-ray luminosity. Furthermore, lines with very low critical densities like the C I and C II fine structure lines (see Table 3) are also very sensitive to conditions in the outer regions of the disk, where densities are small. These regions are preferentially illuminated by the interstellar (or intracluster) radiation fields which are not included in our current simulations.

Unfortunately, Table 1 is not yet complete, as reliable collision strengths were not available for all species, and a number of less abundant elements were omitted from our calculations in order to limit computational costs. In particular, the following species were not included, due to lack of atomic data: Ne I, Mg III, Si I, S I, Fe I, Fe IV, Fe IX, Fe XI, Fe XIII. Due to its complexity, the Fe II ion was also omitted from the present calculations but will be included in future models.

A further observational complication lies in the difficulty in separating the emission from the disk, the wind, the accretion funnels and the photosphere. High resolution spectroscopy offers one possibility, in which line profiles that are shifted and/or broadened to different extents in the different emission regimes can be resolved (e.g. Herczeg et al., 2007). Following the suggestion in MGN08, in future work we will present predicted profiles for a number of potentially observable lines emitted from different regions of the disk. An alternative way to distinguish lines formed in the upper layers of the disk and those formed in the accretion funnel would involve a comparison of transitions with different critical densities (e.g. O 16302 with $N_{crit} = 1.5 \times 10^6\text{ cm}^{-3}$, compared to O 163 μm with $N_{crit} = 2 \times 10^4\text{ cm}^{-3}$).

We note that some of our predicted line intensities differ somewhat from those calculated by MGN08. In most cases, the differences may be explained by the fact that our work used a different disk model for the underlying gas density distribution, and different gas abundances. By way of comparison, we have also computed a model that uses the same input parameters and disk model as those of MGN08 and we compare the predicted line fluxes to those of MGN08 in Table 3. Most of the lines listed are in reasonable agreement, particularly when one considers the two different approaches to the problem and the use of different atomic data. MGN08 predict larger [Ne II] $12.8\mu\text{m}$ line luminosities than in our model; this is

explained by the fact that MGN08 do not include cooling by [Ne II] line, which, as already noted by Gorti & Hollenbach (2008) is found to be important. As a consequence the gas temperature in the [Ne II] emitting region will be higher in MGN08’s calculations, producing a larger [Ne II] $12.8\mu\text{m}$ luminosity. The C II fine-structure line at $158\mu\text{m}$ shows a larger discrepancy and deserves further attention. Because the critical density of this line is low (see Table 3), it will be collisionally quenched at even modest depths into the disk, and will be preferentially emitted in the less dense upper layers of the disk corona. MGN08 calculations, however, were focused on the characterisation of lower layers in the disk and stopped short of the corona, with the result that some of the flux from the C II bright regions is probably missed.

A detailed comparison of the line luminosities predicted by Gorti & Hollenbach (2008) to those predicted by our models is hindered by the different parameters and approaches employed by the two models. However we note that the [Ne II] $12.8\mu\text{m}$ luminosity predicted by our models is a factor of 3.3 lower than that derived by their fiducial model (Model A, their Table 4). This can be explained by the fact that our density distribution is determined by the dust temperature structure. Indeed Gorti & Hollenbach (2008) comment that when they assume a dust-determined temperature structure they obtain a factor of ~ 4 lower [Ne II] line luminosities. We also note that our predicted C I and C II fine-structure lines are higher by a factor of ~ 2 than those given by model A in Gorti & Hollenbach (2008). As discussed above, these lines have low critical densities and are therefore extremely sensitive to the details of the density distribution in the emitting region, furthermore, we use a factor of ~ 3 higher elemental abundance for C. These two factors are probably responsible for the small discrepancy at hand. Gorti & Hollenbach (2008) use highly depleted values for the Si elemental abundance; this is the likely cause of the lower (factor of ~ 10) Si II $35\mu\text{m}$ line luminosities predicted by their models. Finally the factor of ~ 3 lower O abundance used in their model is probably one of the causes of the small (factor of ~ 1.5) discrepancy with the O I $63\mu\text{m}$ line luminosity.

5. DISK DISPERSAL BY PHOTOEVAPORATION

Circumstellar disks are observed around the majority of young stars at $\sim 10^6$ yr (e.g. Lada & Lada 2003). By ages of $\sim 10^7$ yr, however, only low-mass debris disks are generally observed (e.g. Manning & Sargent, 1997; Wyatt, Dent & Greaves, 2003), implying disk lifetimes of up to a few $\sim 10^6$ yr. Indeed, recent observations indicate that about 90% of low mass stars lose their primordial disks at 5-7 Myr (e.g. Haisch et al., 2001; Hartmann, 2005; Hernández et al., 2007a). However, very few observations exist of objects in transition between classical T Tauri stars, which still have disks of a few percent of a solar mass, and weak-lined T Tauri stars, which have dispersed nearly all of their circumstellar disks. For example, Hernandez et al. (2007b) reported only a 10% frequency of transitional disk candidates among the disk-bearing low mass stars in their *Spitzer* observations of the Orion OB1 association. This suggests that the mechanism responsible for the final stages of disk dispersal must operate on relatively short timescales—perhaps as short as $\sim 10^5$ yr (e.g. Duvert et al., 2000, Andrews &

Williams, 2005).

Photoevaporative heating from both the central star and external sources has been posited as a viable mechanism able to satisfy the two-timescale nature of the problem. A dramatic illustration of the latter is the apparent photoevaporation of Orion “proplyds” in the vicinity of OB stars (e.g. Johnstone et al. 1998, Adams et al., 2004; Fatuzzo & Adams, 2008). Evidence is also accumulating that disk loss is more rapid in more O-star rich clusters, as judged from observed disk frequencies in low-mass stars (e.g. Albacete-Colombo et al. 2007, Guarcello et al. 2007, Mayne et al. 2007). We will return to photoevaporation by external sources of radiation in future work, and concentrate here on the effect on the disk of irradiation by the central T Tauri star.

Photoevaporation by ultraviolet (UV) radiation from the central star has been investigated by a number of authors (see Alexander, 2007; Dullemond et al, 2007; Hollenbach, Yorke & Johnstone, 2000, for recent reviews). The original models did not couple photoevaporation with viscous evolution, resulting in disk dispersal timescales exceeding the observational estimates. Subsequently, the ‘UV switch’ model of Clarke et al. (2001), which coupled photoevaporative mass loss to viscous evolution, was able to reproduce the two-timescale behaviour implied by the observations. However a number of problems still remain, as pointed out in Clarke et al. (2001). In particular, current models require that the Lyman continuum emission from the central star does not derive from accretion, an issue that is currently unclear (ACP04). X-ray ionisation and heating of the disk corona provide an attractive alternative engine to drive photoevaporative flows. The fact that weak-line T Tauri stars, for which accretion has nearly ceased, are known to be brighter in the X-ray than classical T-Tauri stars, which are still accreting, suggests that the production of X-ray is not linked to accretion. ACP04 estimated an upper limit to the mass-loss driven by X-rays and found it to be at best only comparable to that derived for ultraviolet evaporation. They concluded, therefore, that X-ray heating is unlikely to be the dominant disk dispersal mechanism. ACP04 took into account the effects of X-ray photoionisation and heating on the hydrostatic structure of a typical T Tauri circumstellar disk, but were limited by the fact that the radiative transfer problem could not be solved self-consistently in 2D.

While our models do not yet iterate over the disk density structure, which would be undoubtedly modified by X-ray irradiation, we do calculate the irradiated thermal structure in 2D. It is therefore worthwhile to provide an estimate of the mass-loss rates and dispersal timescales implied by our models. We estimate mass-loss rates by locating, at each radial distance, the base of the photoevaporative flow, defined as the height where the local gas temperature exceeds the escape temperature of the gas, defined as $T_{es} = Gm_H M_*/kR$, where M_* is the stellar mass, R is the radial distance. This height is illustrated as a function of radial distance in Figure 6. The figure shows that, between 8 and 40 AU, the height of the photoevaporating envelope follows a nearly linear increase with radial distance from the star (slope ~ 0.9). To a first approximation, the mass loss rate per unit area can be estimated as $\dot{\Sigma}_x = \rho c_s$, where ρ and c_s are, respec-

tively, the gas density and the sound speed evaluated at the base of the flow.

Figure 7 (left panel) shows $\dot{\Sigma}_X$, the mass loss rate per unit area and (right panel) the mass loss rate from an infinitely thin annulus as a function of radial distance in the disk. $\dot{\Sigma}_X$ peaks at approximately 12 AU, near the gravitational radius, r_g for gas with sound speed of $\sim 7 \text{ km/s}$ ($T \sim 6000 \text{ K}$). We use the definition of r_g given by Hollenbach et al. (1994), where $r_g = GM_*/c_s$. The value at the peak is $3.1 \times 10^{-12} \text{ g s}^{-1} \text{ cm}^{-2}$, this is about a factor of ten higher than the estimate of ACP04 ($2.6 \times 10^{-13} \text{ g s}^{-1} \text{ cm}^{-2}$) and the value obtained by Hollenbach et al. (1994) for UV photoevaporation ($3.9 \times 10^{-13} \text{ g s}^{-1} \text{ cm}^{-2}$). We note that both studies considered the case of a $1 M_\odot$ star; however, since photoevaporation rates scale only weakly with mass ($\sim M^{0.5}$ for EUV photoevaporation and almost linearly for X-ray photoevaporation), this is not sufficient to explain the order of magnitude difference with our rates. As discussed in the next section, our model has a number of limitations which may result in uncertainties in the derived photoevaporation rates. Taking into account statistical uncertainties in the calculated temperatures alone, we find that our models are also consistent with peak values as low as $\sim 8 \times 10^{-13} \text{ g s}^{-1} \text{ cm}^{-2}$, only a factor of ~ 4 higher than previous estimates when corrected for the different stellar masses.

The effects of X-ray photoevaporation are only significant between 8 and 40 AU. There is also a small inner region between 0.03 and 0.16 AU, where, in spite of the large escape temperatures, the intense X-ray field causes the disk to lose mass at a rate of $3\text{-}4 \times 10^{-13} \text{ g s}^{-1} \text{ cm}^{-2}$. Given the small area at small radii, this does not contribute significantly to the mass loss. The reason for the mass loss being mainly concentrated between 8-40 AU is that this region lies far enough from the central star for the escape temperatures to become sufficiently low and not so far that the effects of X-ray irradiation become unimportant. In other words, the steep drop in $\dot{\Sigma}_X$ inside 8 AU corresponds to the location where the sound speed at $\sim 10^4 \text{ K}$ drops below the Keplerian speed. Any mass loss at smaller radii comes from coronal gas. In fact, for radial distances smaller than 8 AU, there is also a thin layer of gas in the disk corona where X-ray irradiation causes temperatures to rise above the local escape temperatures. However, the contribution of this region to the total mass loss budget is negligible. We also note here that by analogy with the X-ray heated accretion disk models of Begelman, McKee and Shields (1983) the wind region might extend inward to about one tenth of the radius where the sound speed equals the escape speed. In that case the wind in Figure 7 would begin at about 0.8 AU and the total mass loss rate would be increased. More recent works by Liffman (2003) and Font et al. (2004) also find that an EUV-driven wind is launched from well inside the gravitational radius (as defined by Hollenbach et al., 1994).

The dispersal timescale implied by our model is of a few Myr, for a $0.027 M_\odot$ disk, and the total mass loss rate is of the order of $\dot{M}_X \sim 10^{-8} M_\odot \text{ yr}^{-1}$. The disk however, as well as being photoevaporated, is also accreting. Therefore, we can assume that the effects of X-ray photoevaporation would not be felt until its vis-

cous accretion rate, \dot{M}_{acc} , has fallen below \dot{M}_X , at which point the disk would empty rapidly within 10-20 AU. Understanding the later evolution of the disk, after the region within 10-20 AU has been emptied, requires us to determine whether the disk beyond $\sim 20 \text{ AU}$ (I) has to accrete in to the 10-20 AU region and then be photoevaporated or (II) is more or less fixed in density profile and then overtaken by the outward propagating ring of mass loss. Behaviour of type I (or II) results if the mass loss rate increases (decreases) as the hole size increases. This question will be answered in a following study where we plan to solve for the density structure and the 2D X-ray transport self-consistently.

Our current calculations give $\dot{M}_X \sim 10^{-8} M_\odot \text{ yr}^{-1}$, implying that disks with $\dot{M}_{acc} \leq 10^{-8} M_\odot \text{ yr}^{-1}$ should disperse rapidly and therefore be seldom observed. However this is in disagreement with observations of a considerable number of systems in the $0.5\text{-}1 M_\odot$ range that are reported to have accretion rates lower than $10^{-8} M_\odot \text{ yr}^{-1}$. Indeed accretion rates as low as $10^{-9} M_\odot \text{ yr}^{-1}$ are seen in the $-0.2 < \log M_* < 0$ mass bin in Figure 8 of Gregory et al. (2006), which, collecting data from a number of authors, shows the correlation between observed mass accretion rates and stellar mass. This indicates that our predicted $\dot{M}_X \sim 10^{-8} M_\odot \text{ yr}^{-1}$ is probably too high, and may point to a weakness of our model (see discussion in the next Section).

5.1. Limitations of our models

A number of important approximations were used in our models, which may lead to uncertainties in the estimates of the photoevaporation rates.

One major caveat of our model, already mentioned in this paper, is that the influence of X-ray photoionisation and heating on the disk density structure has been ignored. The high gas temperatures reached in the inner regions of the disk would cause an expansion of the gas in the z-direction, as shown, for example, by ACP04. Indeed, their lower value of mass loss rate is perhaps caused by a larger attenuation of the X-ray field due to the 'puffed up' inner disk material that is not accounted for by our models. A hot and inflated inner disk could in fact cause a shadowing effect of the regions at larger radial distances, reducing the effects of X-ray photoevaporation there. The magnitude of this effect can only be properly estimated via the simultaneous solution of the 2D radiative transfer problem and the 1D hydrostatic equilibrium in the z-direction, which is the aim of a follow-up paper.

Further uncertainties are introduced by the use of the " $\rho \times c_s$ " approximation in the calculation of photoevaporation rates. In Section 5 we discuss how the base of the photoevaporative envelope is defined as the height where the local gas temperature exceeds the escape temperature of the gas. While this is generally a very good approximation in cases where the temperature and density vary sharply at the ionisation front, as for EUV photoevaporation (e.g. Hollenbach et al., 1994), in the case of X-ray photoevaporation presented here, the distinction between the bound and unbound gas is less clear. In other words, a small error in the determination of temperatures in our models, would lead to much larger uncertainties in the density, and hence in the estimated

photoevaporation rates.

We conclude that while we have shown that X-rays have the potential to drive an outflow, our derived rates should be treated with caution and we defer firm conclusions to future work.

6. SUMMARY

We have presented a 2D photoionisation and dust radiative transfer calculation of a typical T Tauri protoplanetary disk irradiated by 1.5×10^7 K ($kT = 1.36$ keV) X-ray radiation field from the central pre-main sequence star.

A detailed characterisation of the temperature structure of the upper disk corona was provided, which uncovered the existence of a layer of highly ionised, hot gas in the inner disk regions. The maximum temperatures reached by the gas in the upper corona were mapped across the radial dimension of the disk, showing peaks exceeding 10^6 K in the very inner regions. The hotter component of the gas in the inner disk and at radii between ~ 8 to ~ 40 AU was shown to be unbound, and probably part of a photoevaporative flow.

To aid future efforts to observe the hot/warm gas component of T Tauri disks, we provide a substantial list of predicted emission line luminosities, many of which should already be detectable with current instrumentation.

The temperature structure of the irradiated disk im-

plies a total mass loss rate of $\sim 10^{-8} M_{\odot} \text{ yr}^{-1}$ and a disk dispersal timescale of a few Myr for a disk mass of $0.027 M_{\odot}$, which is the mass of the disk structure model we employed. We discuss the limitations of our model and highlight the need for further calculations that solve the 2D radiative transfer problem simultaneously with the 1D hydrostatic equilibrium of disk structure in the polar direction.

ACKNOWLEDGMENTS

We extend our warmest thanks to Al Glassgold, for insightful discussion and a thorough assessment of our results. We also thank the anonymous referee and the editor Eric Feigelson for helpful comments that added to the clarity of the paper and the interpretation of the results. We thank Paola D'Alessio for providing us with the electronic data for the gas density distribution in the disk. We also thank Bruce Draine for help with the X-ray dust opacity calculations. We finally extend our thanks to Roger Wesson for helpful discussion. JJD was supported by the Chandra X-ray Center NASA contract NAS8-39073 during the course of this research. BE was partially supported by *cChandra* grants GO6-7008X and GO6-7009X. The simulations were partially run on the Cosmos (SGI altix 4700) supercomputer at DAMTP in Cambridge. Cosmos is a UK-CCC facility which is supported by HEFCE and STFC.

REFERENCES

- Adams, F. C., Hollenbach, D., Laughlin, G., & Gorti, U. 2004, *ApJ*, 611, 360
- Akeson, R. L., et al. 2005, *ApJ*, 622, 440
- Albacete Colombo, J. F., Flaccomio, E., Micela, G., Sciortino, S., & Damiani, F. 2007, *A&A*, 464, 211
- Alexander, R. 2007, ArXiv e-prints, 712, arXiv:0712.0388
- Alexander, R. D., Clarke, C. J., & Pringle, J. E. 2004, *MNRAS*, 354, 71, ACP04
- Andrews, S. M., & Williams, J. P. 2007, *ApJ*, 659, 705
- Asplund, M., Grevesse, N., & Sauval, A. J. 2005, *Cosmic Abundances as Records of Stellar Evolution and Nucleosynthesis*, 336, 25
- Ayres, T. R., Plymate, C., & Keller, C. U. 2006, *ApJS*, 165, 618
- Balbus, S. A., & Hawley, J. F. 1991, *ApJ*, 376, 214
- Bally, J., Sutherland, R. S., Devine, D., & Johnstone, D. 1998, *AJ*, 116, 293
- Begelman, M. C., McKee, C. F., & Shields, G. A. 1983, *ApJ*, 271, 70
- Clarke, C. J., & Pringle, J. E. 2006, *MNRAS*, 370, L10
- Clarke, C. J., Gendrin, A., & Sotomayor, M. 2001, *MNRAS*, 328, 485
- D'Alessio, P., Canto, J., Calvet, N., & Lizano, S. 1998, *ApJ*, 500, 411
- D'Alessio, P., Calvet, N., & Hartmann, L. 2001, *ApJ*, 553, 321
- D'Alessio, P. 2003, *Revista Mexicana de Astronomia y Astrofisica Conference Series*, 18, 14
- Drake, J. J., & Testa, P. 2005, *Nature*, 436, 525
- Dullemond, C. P., van Zadelhoff, G. J., & Natta, A. 2002, *A&A*, 389, 464
- Dullemond, C. P., Hollenbach, D., Kamp, I., & D'Alessio, P. 2007, *Protostars and Planets V*, 555
- Duvert, G., Guilloteau, S., Ménard, F., Simon, M., & Dutrey, A. 2000, *A&A*, 355, 165
- Ercolano, B., Barlow, M. J., Storey, P. J., & Liu, X.-W. 2003a, *MNRAS*, 340, 1136
- Ercolano, B., Barlow, M. J., & Storey, P. J. 2005, *MNRAS*, 362, 1038
- Ercolano, B., & Storey, P. J. 2006, *MNRAS*, 372, 1875
- Ercolano, B., Young, P. R., Drake, J. J., & Raymond, J. C. 2008, *ApJS*, 175, 534
- Espaillet, C., et al. 2007, *ApJ*, 664, L111
- Evans, N. J., II, et al. 2003, *PASP*, 115, 965
- Fatuzzo, M., & Adams, F. C. 2008, *ApJ*, 675, 1361
- Font, A. S., McCarthy, I. G., Johnstone, D., & Ballantyne, D. R. 2004, *ApJ*, 607, 890
- Glassgold, A. E., Najita, J., & Igea, J. 2004, *ApJ*, 615, 972, GNI04
- Glassgold, A. E., Feigelson, E. D., Montmerle, T., & Wolk, S. 2005, *Chondrites and the Protoplanetary Disk*, 341, 165
- Glassgold, A. E. 2006, *Proceedings of the NASA LAW 2006*, held February 14-16, 2006, UNLV, Las Vegas. Published by NASA Ames, Moffett Field, CA, 2006., p.34, 34
- Glassgold, A. E., Najita, J. R., & Igea, J. 2007, *ApJ*, 656, 515
- Gregory, S. G., Jardine, M., Simpson, I., & Donati, J.-F. 2006, *MNRAS*, 371, 999
- Grevesse, N., & Sauval, A. J. 1998, *Space Science Reviews*, 85, 161

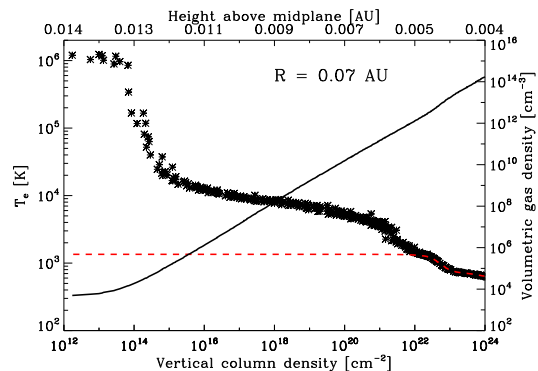


FIG. 1.— Gas temperature structure (asterisks) as a function of gas column depth in the disk atmosphere at a radial distance of 0.07 AU. The dust temperature distribution of D'Alessio et al. (1999) is plotted as the red dashed line. The black solid line shows the volumetric gas density [cm^{-3}] as a function of depth.

TABLE 1
COLLISIONALLY EXCITED LINES IN ORDER OF DECREASING LINE LUMINOSITY. THE FLUX AT A DISTANCE D , ASSUMING A FACE ON ORIENTATION OF THE DISK, IS OBTAINED BY DIVIDING THE LINE LUMINOSITIES BY $4\pi D^2$.

Species	Wavelength [Å]	Luminosity [L_{\odot}]	Species	Wavelength [Å]	Luminosity [L_{\odot}]
MgI	4573.18	3.3e-05	SiII	335008.	6.1e-08
SiII	348189.	1.4e-05	MgIV	44883.3	5.8e-08
OI	631712.	6.1e-06	OI	5578.89	5.5e-08
OI	6302.03	3.5e-06	SiII	2335.32	5.0e-08
MgII	2796.35	2.6e-06	NI	10400.6	4.2e-08
MgI	2852.14	1.6e-06	OIII	518135.	4.1e-08
MgII	2803.53	1.3e-06	CII	2328.84	3.9e-08
OI	6365.53	1.1e-06	SiII	2344.92	3.5e-08
SiII	4069.76	1.0e-06	CII	2325.40	3.3e-08
CII	1.57729e+06	9.6e-07	OIII	5008.24	3.2e-08
CI	9852.99	9.5e-07	CI	2968.08	3.0e-08
SiII	6732.69	8.7e-07	SiII	9070.05	2.9e-08
NeII	128156.	8.7e-07	NII	6549.86	2.7e-08
CI	8729.51	4.6e-07	CII	2324.21	2.4e-08
SiII	6718.31	4.1e-07	NI	10410.5	2.1e-08
CI	3.70370e+06	3.9e-07	FeXIII	10746.2	1.9e-08
CI	9826.85	3.2e-07	OII	3727.09	1.9e-08
OI	1.45560e+06	3.0e-07	OIII	883392.	1.8e-08
SiII	10323.3	2.9e-07	NI	10410.0	1.8e-08
SiII	4077.51	2.7e-07	FeVI	147710.	1.6e-08
SiII	10289.5	2.6e-07	FeVI	195580.	1.6e-08
CII	2326.11	1.9e-07	NI	3467.49	1.4e-08
SiII	10339.2	1.8e-07	NIII	573394.	1.3e-08
SiIII	9532.25	1.6e-07	NI	10401.1	1.3e-08
NeIII	155545.	1.5e-07	CI	2965.70	1.3e-08
SIV	105108.	1.4e-07	SiII	1816.93	1.2e-08
CI	6.09756e+06	1.3e-07	NeIII	3869.85	1.2e-08
MgI	4564.67	9.6e-08	FeXI	60823.6	1.2e-08
SiII	187056.	8.4e-08	FeXI	2649.46	1.1e-08
NII	6585.27	8.4e-08	SiII	2335.12	1.1e-08
SiII	10373.3	7.3e-08	OIII	4960.29	1.1e-08
CII	2327.64	7.3e-08	FeVI	123107.	1.0e-08

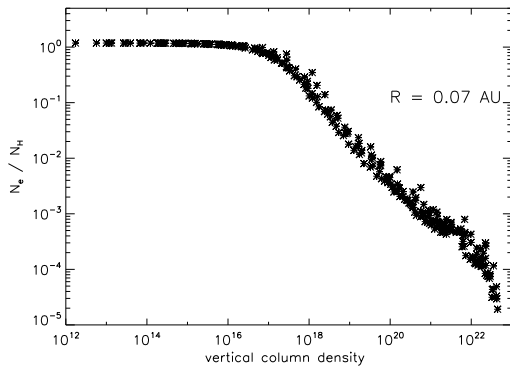


FIG. 2.— Fractional abundance of electrons with respect to hydrogen nuclei plotted as a function of depth in the disk atmosphere at a radial distance of 0.07 AU.

Guarcello, M. G., Prisinzano, L., Micela, G., Damiani, F., Peres, G., & Sciortino, S. 2007, *A&A*, 462, 245
 Güdel, M., Skinner, S. L., Briggs, K. R., Audard, M., Arzner, K., & Telleschi, A. 2005, *ApJ*, 626, L53
 Haisch, K. E., Jr., Lada, E. A., & Lada, C. J. 2001, *ApJ*, 553, L153
 Hartmann, L. 2005, *Chondrites and the Protoplanetary Disk*, 341, 131
 Hatchett, S., Buff, J., & McCray, R. 1976, *ApJ*, 206, 847
 Herczeg, G. J., Najita, J. R., Hillenbrand, L. A., & Pascucci, I. 2007, *ApJ*, 670, 509

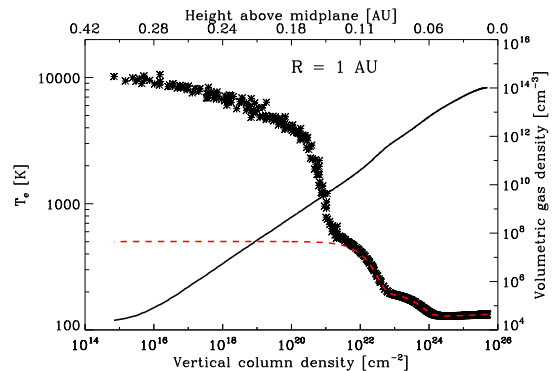


FIG. 3.— Gas temperature structure (asterisks) as a function of depth in the disk atmosphere at a radial distance of 1 AU. The dust temperature distribution of D'Alessio et al. (1999) is plotted as the red dashed line. The black solid line shows the volumetric gas density [cm^{-3}] as a function of depth.

Hernández, J., et al. 2007a, *ApJ*, 662, 1067
 Hernández, J., et al. 2007b, *ApJ*, 671, 1784
 Hollenbach, D. J., Yorke, H. W., & Johnstone, D. 2000, *Protostars and Planets IV*, 401
 Hollenbach, D., & McKee, C. F. 1979, *ApJS*, 41, 555
 Hollenbach, D., Johnstone, D., Lizano, S., & Shu, F. 1994, *ApJ*, 428, 654
 Igea, J., & Glassgold, A. E. 1999, *ApJ*, 518, 848

TABLE 2
HYDROGEN RECOMBINATION LINES THE FLUX AT A DISTANCE D , ASSUMING A FACE ON ORIENTATION OF THE DISK, IS OBTAINED BY DIVIDING THE LINE LUMINOSITIES BY $4\pi D^2$.

Transition	Wavelength [Å]	Luminosity [L_{\odot}]	Transition	Wavelength [Å]	Luminosity [L_{\odot}]
2-1	1215.68	3.0e-05	9-2	3836.51	1.2e-07
3-2	6564.70	2.6e-06	9-3	9231.60	4.0e-08
4-2	4862.74	9.5e-07	9-4	18179.2	1.7e-08
4-3	18756.3	3.2e-07	10-2	3799.01	1.0e-07
5-2	4341.73	4.7e-07	10-3	9017.44	3.3e-08
5-3	12821.7	1.6e-07	10-4	17366.9	1.4e-08
5-4	40522.8	7.8e-08	11-2	3771.74	9.6e-08
6-2	4102.94	2.9e-07	11-3	8865.27	2.9e-08
6-3	10941.2	9.8e-08	11-4	16811.2	1.2e-08
6-4	26258.8	4.6e-08	12-2	3751.25	8.5e-08
6-5	74598.8	2.5e-08	12-3	8752.93	2.6e-08
7-2	3971.24	2.0e-07	12-4	16411.7	1.1e-08
7-3	10052.2	6.7e-08	13-2	3735.47	7.7e-08
7-4	21661.3	3.1e-08	13-3	8667.45	2.3e-08
7-5	46537.9	1.6e-08	13-4	16113.8	1.0e-08
7-6	123719.	9.8e-09	14-2	3723.03	6.8e-08
8-2	3890.19	1.5e-07	14-3	8600.81	2.1e-08
8-3	9548.65	5.0e-08	14-4	15884.9	9.1e-09
8-4	19450.9	2.2e-08	15-2	3713.06	6.1e-08
8-5	37405.7	1.2e-08	15-3	8547.78	1.8e-08
			15-4	15705.0	8.1e-09

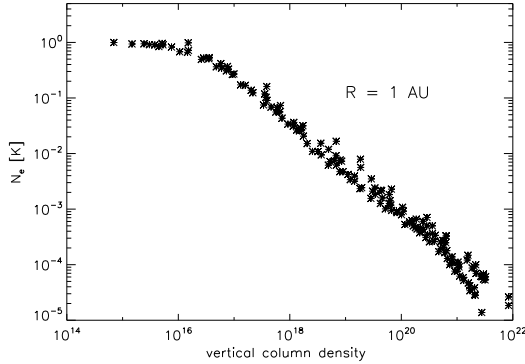


FIG. 4.— Fractional abundance of electrons with respect to hydrogen nuclei plotted as a function of depth in the disk atmosphere at a radial distance of 1 AU.

TABLE 3

COMPARISON OF PREDICTED LINE LUMINOSITIES WITH MGN08

Species	Wavelength [Å]	N_{crit} [cm^{-3}]	Luminosity [L_{\odot}]	
			This Work	MGN08
OI	631712.	2.1e4	2.2e-05	3.8e-05
CI	6.09756e+06	1.7e0	8.5e-06	2.6e-07
CI	3.70370e+06	9.5e0	8.2e-06	9.2e-07
OI	6302.03	1.5e6	7.7e-06	7.5e-06
CII	1.57729e+06	4.9e1	3.0e-06	5.6e-09
CII	2326.11	1.4e9	1.1e-06	1.0e-06
NeII	128156.	5.9e5	9.5e-07	3.7e-06
CI	9826.85	1.4e4	8.9e-07	3.7e-06
OI	5578.89	9.5e7	4.9e-07	4.2e-07
NeIII	155545.	2.0e5	1.9e-07	4.2e-07

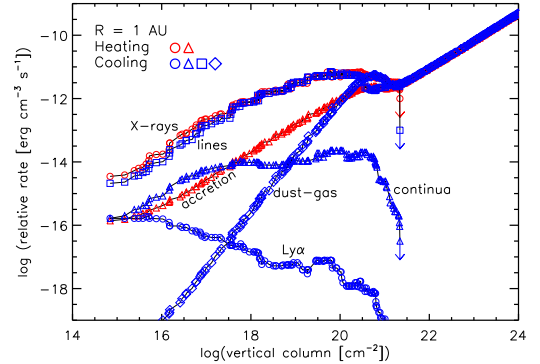


FIG. 5.— Thermal balance as a function of depth in the disk atmosphere at a radial distance of 1 AU. The jaggedness of the lines is due to Monte Carlo statistical error. Please refer to the online version of this paper for a colour figure. Red circles: heating by X-ray photoionisation; red triangles: heating by viscous accretion; blue circles: cooling by $Ly\alpha$ emission; blue triangles: cooling by free-free and free-bound continuum emission from hydrogen and helium; blue squares: cooling by collisionally excited lines of metals; blue diamonds: cooling by dust-gas collisions.

- Johnstone, D., Hollenbach, D., & Bally, J. 1998, *ApJ*, 499, 758
Kashyap, V., & Drake, J. J. 2000, *Bulletin of the Astronomical Society of India*, 28, 475
Kastner, J. H., Huenemoerder, D. P., Schulz, N. S., Canizares, C. R., & Weintraub, D. A. 2002, *ApJ*, 567, 434
Keene, J., & Masson, C. R. 1990, *ApJ*, 355, 635
Kwan, J. 1997, *ApJ*, 489, 284
Kwan, J., & Tademaru, E. 1988, *ApJ*, 332, L41
Kwan, J., & Tademaru, E. 1995, *ApJ*, 454, 382
Lada, C. J., & Lada, E. A. 2003, *ARA&A*, 41, 57
Landi, E., & Phillips, K. J. H. 2006, *ApJS*, 166, 421
Laor, A., & Draine, B. T. 1993, *ApJ*, 402, 441
Lahuis, F., van Dishoeck, E. F., Blake, G. A., Evans, N. J., II, Kessler-Silacci, J. E., & Pontoppidan, K. M. 2007, *ApJ*, 665, 492
Liffman, K. 2003, *Publications of the Astronomical Society of Australia*, 20, 337

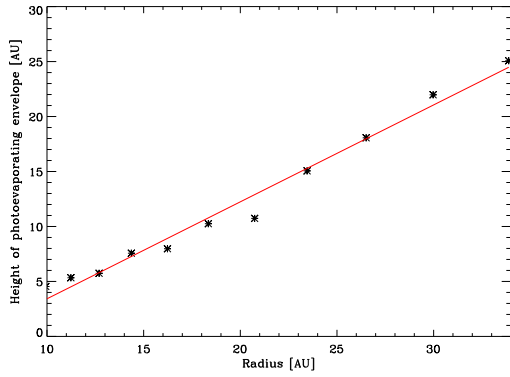


FIG. 6.— Height of the photoevaporative envelope traced across the major photoevaporation region. The slope of line relating this quantity to the radial distance is 0.9.

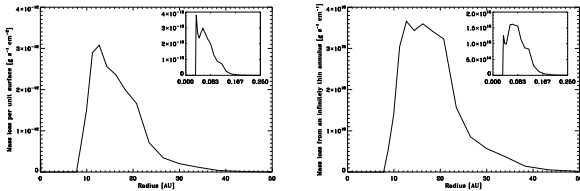


FIG. 7.— Left: Mass loss per unit surface area as a function of the radial distance from the central star. Right: Mass loss from an infinitely thin annulus as a function of the radial distance from the central star. The insets show the 0 to 0.3 AU region enlarged for clarity.

Mannings, V., & Sargent, A. I. 1997, *ApJ*, 490, 792

- Mayne, N. J., Naylor, T., Littlefair, S. P., Saunders, E. S., & Jeffries, R. D. 2007, *MNRAS*, 375, 1220
- Mazzotta, P., Mazzitelli, G., Colafrancesco, S., & Vittorio, N. 1998, *A&AS*, 133, 403
- Meijerink, R., Glassgold, A. E., & Najita, J. R. 2007, *ArXiv e-prints*, 712, arXiv:0712.0112, MGN08
- Meyer, M. R., et al. 2004, *ApJS*, 154, 422
- Najita, J. R., Carr, J. S., Glassgold, A. E., & Valenti, J. 2007, *ArXiv e-prints*, 704, arXiv:0704.1841
- Natta, A., Testi, L., & Randich, S. 2006, *A&A*, 452, 245
- Nomura, H., & Millar, T. J. 2005, *A&A*, 438, 923
- O'dell, C. R. 1993, *Science*, 259, 33
- Pascucci, I., et al. 2007, *ApJ*, 663, 383
- Pringle, J. E. 1981, *ARA&A*, 19, 137
- Qi, C., Wilner, D. J., Calvet, N., Bourke, T. L., Blake, G. A., Hogerheijde, M. R., Ho, P. T. P., & Bergin, E. 2006, *ApJ*, 636, L157
- Raymond, J. C. 1993, *ApJ*, 412, 267
- Semenov, D., Wiebe, D., & Henning, T. 2004, *A&A*, 417, 93
- Socas-Navarro, H., & Norton, A. A. 2007, *ApJ*, 660, L153
- Socas-Navarro, H., & Centeno, R. 2008, *ArXiv e-prints*, 803, arXiv:0803.0990
- van Dishoeck, E. F., & Jørgensen, J. K. 2008, *Ap&SS*, 313, 15
- Walter, F. M., & Kuhl, L. V. 1981, *ApJ*, 250, 254
- Wilner, D. J., Bourke, T. L., Wright, C. M., Jørgensen, J. K., van Dishoeck, E. F., & Wong, T. 2003, *ApJ*, 596, 597
- Wyatt, M. C., Dent, W. R. F., & Greaves, J. S. 2003, *MNRAS*, 342, 876